Organ scale nitrogen map: a novel approach for leaf nitrogen concentration estimation

Alexis Carlier[1], Sebastien Dandrifosse[1], Benjamin Dumont[2] and Benoît Mercatoris[1]

[1]Biosystems Dynamics and Exchanges, TERRA Teaching and Research Centre, Gembloux Agro-Bio Tech, University of Liège, 5030 Gembloux, Belgium

[2]Plant Sciences, TERRA Teaching and Research Centre, Gembloux Agro-Bio Tech, University of Liège, 5030 Gembloux, Belgium

Abstract.

Crop nitrogen trait estimations have been used for decades in the frame of precision agriculture and phenotyping. They are crucial information towards a sustainable agriculture and efficient use of resources. Remote sensing approaches are currently accurate tools for nitrogen trait estimations. They are usually quantified through a parametric regression between remote sensing data and the ground truth. For instance, chlorophyll or nitrogen concentrations are accurately estimated using features like vegetation indices. However, those models tend to simplify the observed scene in averaging the features. Thus, they encompass potential other information as the distribution of the concerned trait and tend to underexploit the data.

In this study, we have modeled organ scale nitrogen maps from multispectral camera array images mounted on a ground-based platform. Two wheat fertilization trials were imaged for two years. Reference nitrogen concentration measurements were performed in the laboratory, by taking care to separate the flag leaves from the other leaves. As a single or two nitrogen measurements per image were available, the idea was to exploit the machine learning algorithm capacity to generalize and find patterns. Therefore, small leaf patches were drawn over the images of different nitrogen input objects and growth stages. Patches on the flag leaves and on the other leaves were associated with the corresponding nitrogen measurement. Three machine learning algorithms were trained and tested using features from the six multispectral bands of these patches. The arising patterns, created by the nitrogen changes over the season and nitrogen objects, were used by the model to generate nitrogen maps at the organ scale. It also provided the nitrogen concentration distribution of the observed scene. The percentiles 25 and 75 were the most suitable statistics to predict the leaf and the flag leaf nitrogen concentration with a relative RMSE of 0.11 and 0.15, respectively.

Proceedings of the 15th International Conference on Precision Agriculture
June 26-29, 2022, Minneapolis, Minnesota, United States

2

Introduction

Nitrogen is an essential macronutrient for plants as the major component of chlorophyll and protein ensuring crop production and quality. Its natural availability is not important enough to cover the crop needs. Farmers often fertilize according to a fertilization program which might generate over or under-fertilization. It can cause nitrogen pollution, a drop in crop yield or increase the probability of lodging. In this sense, breeders are trying to overcome the challenge of limiting the crop nitrogen demand while increasing yield through the evaluation of the nitrogen use efficiency (NUE) (Cormier et al., 2016; Hawkesford & Riche, 2020). As a complex trait including many processes, improving NUE is not trivial and requires a lot of data. Most of these traits are dependent on genetics (G), environment (E), and management (M) and their interactions (G x E x M) (Hawkesford & Riche, 2020). For example, (Barraclough et al., 2014) described significant genetic variation in N contents of individual organs. Plant breeding is a tedious work where there is a real need for high-throughput data acquisition systems.

Phenotyping methods are becoming mainstream tools that provide relevant traits for farmers as well as for breeders or researchers in a high-throughput and objective way (Reynolds et al., 2020; Weiss et al., 2020). Satellite imaging is mainly dedicated to farmers for nitrogen monitoring as it provides spatially and temporally consistent information over the growing season. On the other hand, ground-based phenotyping platforms are mostly used in the frame of breeding or research which needs more details. Other vectors such as airborne or UAV might be used in both cases. The main embedded technology used for nitrogen level estimation is spectroscopy (Verrelst et al., 2019). The underlying idea mainly relies on the strong but brittle correlation between nitrogen content and chlorophyll content which demonstrates strong and specific light absorption bands in the visible domain (Gitelson et al., 2003, Berger et al., 2020). The most common and simplest spectroscopy data processing is the use of vegetation indices. Many of them correlate well with chlorophyll content (Cammarano et al., 2014; Padilla et al., 2018; Prey & Schmidhalter, 2019). Other methods use radiative-transfer models to quantify biophysical variables (Verrelst et al., 2019).

To our knowledge, all approaches, except clip leaf measurements, compared one average nitrogen value, i.e. leaf nitrogen content or plant nitrogen content, with a single or an average spectrum of the observed scene. However, nitrogen is not evenly distributed and is redistributed all along the season. Moreover, at the canopy scale, the measured reflectance is a function of not only biophysical variables but also of the soil background and the canopy structural properties. That is why we proposed a novel approach to visualize nitrogen concentration partitioning of a wheat canopy. It uses multispectral images to model a crop nitrogen map at the pixel level using machine learning algorithms.

Materials and methods

In field and image data acquisition

Data was acquired for two seasons, 2020 and 2021, in trials located in the Hesbaye area, Belgium. Winter wheat was sown in microplots of 1.95 m large and 6 m long with a row spacing of 0.14 m on homogenous deep silt loam soil and a temperate climate. The microplots were fertilized three times at BBCH growth stages (GS) 28, 30, and 39 with 27% ammonium nitrate. Two types of trials were conducted for both years. The first one was a fertilization trial (F) composed of different levels of applied fertilizer from 0 kg/ha to 330kg/ha of nitrogen. The second type of trial was composed of different combinations of fertilization applications associated with different fungicide application programs (FP). Cultivars 'LG Vertikal' and 'Mentor' were sown respectively for FP and F.

Manual measurements were performed on major phenological BBCH GS (see Table 1). Depending on the trial, measurements were done on three or four replicates per trial. Aboveground biomasses were sampled on 0.50 m long on the three central rows. All leaves and

Proceedings of the 15th International Conference on Precision Agriculture
June 26-29, 2022, Minneapolis, Minnesota, United States

3

flag leaves were separated from tillers, weighted, and dried until constant weights. All organs were then sent to a lab for nitrogen concentration determination using the Dumas method.

Table 1, Data acquisitions details of each trial

Trial name	Number of objects	Number of microplots	Camera height above the canopy	BBCH GS – Manual measurements
20-FP	7	21	≃1.60m	38, 65
20-F	5 or 8	20 or 31	≃1.60m	33, 39, 65, 75
21-FP	7	21	≃1.60m	40, 62
21-F	5	20	≃1.60m	30, 32, 39, 65, 75

A phenotyping platform was designed to capture nadir frames of wheat microplots. A sensor pod was installed on a cantilever beam to avoid shadows from the rest of the platform in the images. That sensor pod combined a multispectral camera array with six optical filters centered at 490, 550, 680, 720, 800 and 900 nm, and two RGB cameras used to record color and 3D information by stereovision (Figure 1). The multispectral camera array was a Micro-MCA (Tetracam Inc., Gainesville, FL, USA) and the RGB cameras were the GO-5000C-USB cameras (JAI A/S, Copenhagen, Denmark). This acquisition system and the following pre-processing were detailed in our previous work (Carlier et al., 2022; Dandrifosse et al., 2020). The height of the pod was adjusted at each acquisition date to keep a distance around 1.6 m between the cameras and the top of the canopy. At this distance, the footprint of the frames was approximately 0.98 m^2 for the multispectral camera array and 1.26 m^2 for the RGB cameras. The images were recorded using a color depth of 10 or 12 bits per pixel then reduced to 8 bits per pixel, because the stereovision and the registration open-source libraries need 8-bit inputs. The auto-exposure algorithms of the RGB and multispectral devices were adapted to prevent image saturation. An incident light spectrometer AvaSpec-ULS2048 (Avantes, Apeldoorn, The Netherlands) was positioned above the cameras. A spectrum of the incident sunlight was recorded at each image acquisition using a 16-bit resolution. Each recorded spectrum was the average of three consecutive measurements. It was corrected for dark noise and nonlinearity of pixel response to exposure time. Thanks to the factory calibration, digital values were converted to irradiance data. Each acquisition of images and their associated solar spectrum took only a few seconds. It corresponded to the time necessary to average the spectrums and ensure a proper exposure time for all the cameras.
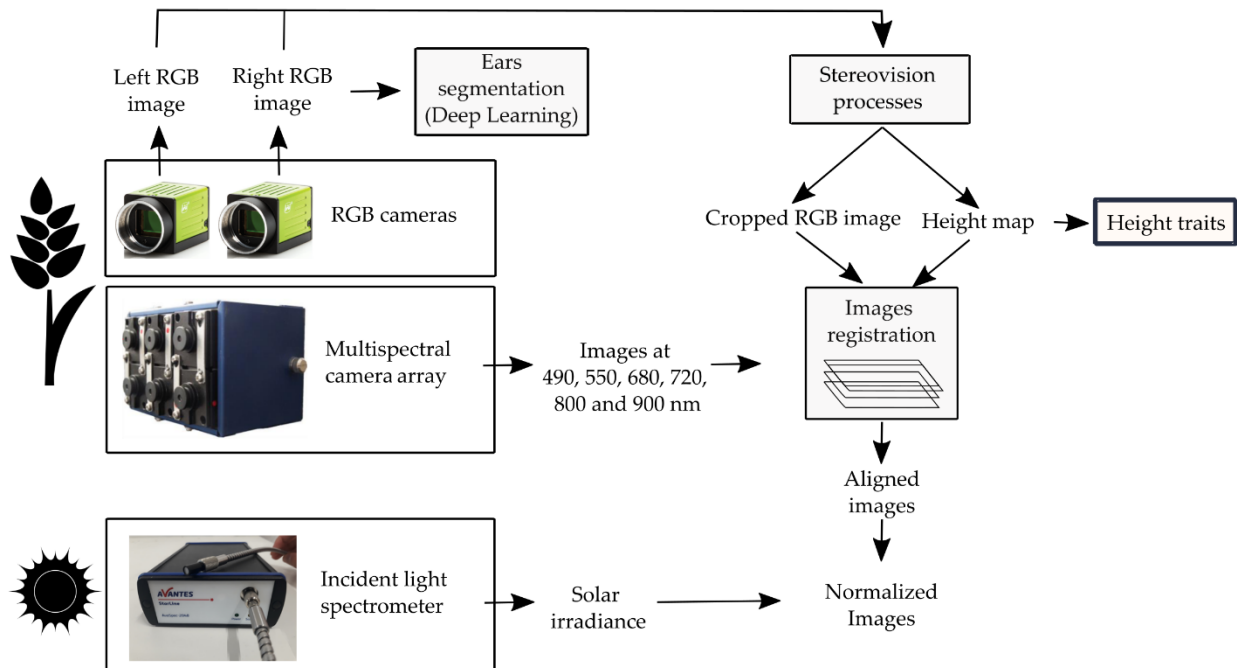
Proceedings of the 15th International Conference on Precision Agriculture
June 26-29, 2022, Minneapolis, Minnesota, United States

4

Figure 1, Data pre-processing workflow

Data processing

Stereovision

A stereovision method has been developed by Dandrifosse et al., (2020) using stereovision functions from OpenCV-Python library (version 4.5.3.56). It exploits the overlaps between the two RGB images. The percentile 95 of the computed canopy height map was used to deduce canopy height in the following image registration process.

Image pre-processing

Owing to the disposition of the cameras and the proximity with the canopy, the different images were not perfectly overlapping. (Dandrifosse et al., 2021) developed a methodology of image registration to align pixel to pixel the six grayscale images from the multispectral camera and the left RGB image (Figure 1). A simple global transformation was first performed to provide roughly registered images. Then, a second more efficient method was used. It is called the B-SPLINE method using the Pyelastix (version 1.2) python library. It uses an area-based method called normalized mutual information metric and performs a local transformation based on a third order B-SPLINE model. Resulting images are cropped to 855 x 594 pixels that correspond to the common scene.

A second pre-processing refers to image normalization to the incident light. A method to calculate an estimation of the bi-directional reflectance factor (BRF) has been developed by (Dandrifosse, Carlier, et al., 2022). It is defined as the ratio of the reflected radiance to the incident irradiance. In other words, it is the ratio between the light measured through the image to the light measured by the incident light spectrometer. This method allowed to correct illumination condition changes encountered across the season. BRF is also known as reflectance in other studies.

Finally, soil-plant and plant-ear segmentations were performed to distinguish between soil, ears, and the rest of the plants. The soil segmentation used the 800 nm channel which shows significant reflectance differences between soil and plant. A method taking the first local minimum in the histogram has been developed that provides a good segmentation. In some cases, with strong direct sunlight, a second threshold was made on the 490 nm channel. Finally, the state-of-the-art deep learning algorithm Yolov5 was used to detect ears associated with the Deep Mac model to get an ear mask (Dandrifosse, Ennadifi, et al., 2022)

Proceedings of the 15th International Conference on Precision Agriculture
June 26-29, 2022, Minneapolis, Minnesota, United States

5

The approach relies on defining pixels belonging to flag leaves and to other leaves for which nitrogen concentration measurements were available. To build the datasets, one image of three contrasted nitrogen objects was selected for each date for the training set and one image of a well fertilized object for the validation dataset. The training and validation datasets were composed of 39 images and 13 images, respectively. For each image, small distinct patches were manually drawn (Figure 2) on the flag leaves and on the other leaves thanks to the online platform Apeer.com. Patches should represent the most possible different situations and light conditions and have the same amount of flag leaf than other leaf patches.
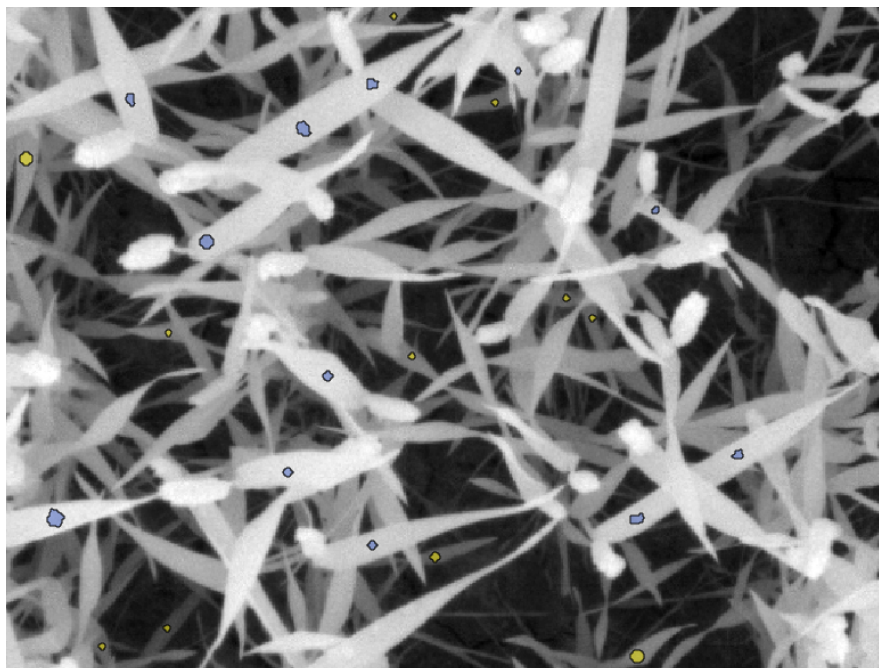

Figure 2, Illustration of the annotation process with flag leaves in blue and the other leaves in yellow on a 800 nm image.

Machine learning training

For each patch, a set of features were extracted in order to be related to the nitrogen concentration. Firstly, the six normalized channels of the multispectral camera were considered to estimate the BRF. Then, a couple of vegetation indices were computed using these BRF images. They were the mNDb (Jay et al., 2017), the GIT1, the GNDVI (A. Gitelson & Merzlyak, 1994), GIT2, GIT3 (A. A. Gitelson et al., 2003), the CIrede, CIgreen (Roujean & Breon, 1995) and the NDRE (Barnes et al., 2000). BRF and vegetation indices values were the average of the pixels belonging to one patch. The growing degree days after sowing was also added as a proxy of the growth stage. Target value of the patch was the nitrogen concentration values given by the laboratory either for flag leaves or for the other leaves. Three machine learning algorithms were tested: random forest (RF), support vector machine (SVM), and K-nearest neighbors (KNN) with default parameters. All developments were made on Python 3.7 with OpenCV 4.5.3.56 and Scikit-learn 0.24.2 libraries. Performances were evaluated on the R^2 and on the relative root mean square error (rRMSE) defined as the RMSE to the average value.

Results

Nitrogen map

Three machine learning algorithms were evaluated on the validation set. Results showed that the random forest slightly outperformed the others with a rRMSE of 0.12 whereas it was 0.14 and 0.13 respectively for KNN and SVM. Applied to every pixel of an image, the model generated

Proceedings of the 15th International Conference on Precision Agriculture
June 26-29, 2022, Minneapolis, Minnesota, United States

6

nitrogen maps as illustrated in Figure 3. It offers a good visualization of the nitrogen concentration partitioning in a wheat canopy. We may for example observe that the leaves at the top of the canopy showed greater values than the leaves at the bottom of the canopy.
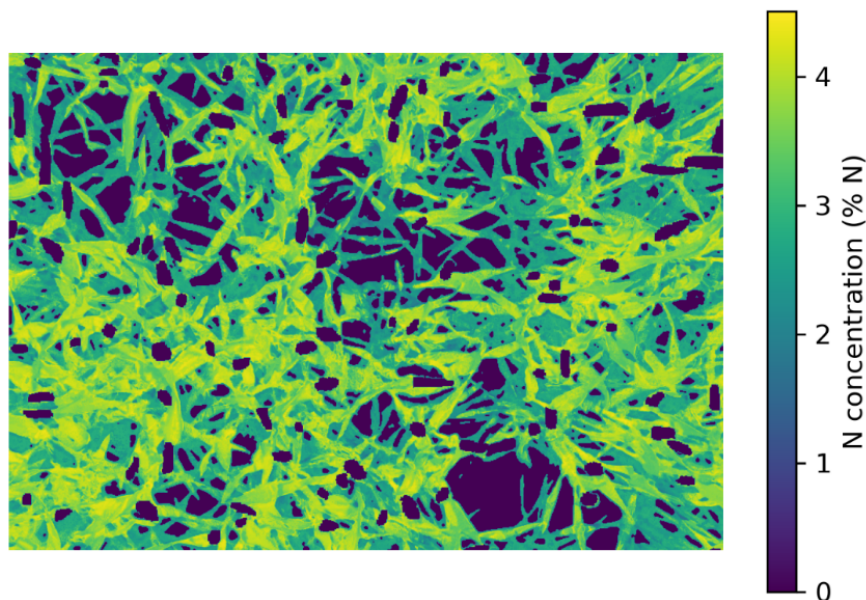

Figure 3, Predicted nitrogen map. Soil and ears are in dark blue.

Leaf nitrogen estimation

The nitrogen map allows us to extract a nitrogen value for each pixel of the map and therefore compute the nitrogen distribution of the observed canopy. Percentile 25, 75 and the average were computed from the nitrogen distribution. The statistic 'average' of the distribution is the reference as it is the usual statistic used in other studies.

Table 2, rRMSE of nitrogen concentration estimation regarding different statistics

Origin	Statistics	All leaves	Other leaves	Flag leaves
Nitrogen map distribution	Percentile 25	0.14	0.15	0.32
	Average	0.14	0.22	0.21
	Percentile 75	0.24	0.35	0.11

The results in Table 2 show that the flag leaves are best predicted by the percentile 75 of the distribution with a clear improvement compared to the average. Concerning the other leaves, the percentile 25 outperforms the other statistics. Finally, the average leaf nitrogen concentration, i.e. all leaves, was best estimated by the average with a R^2 of 0.67 (Figure 4) and the percentile 25 with a R^2 of 0.64.
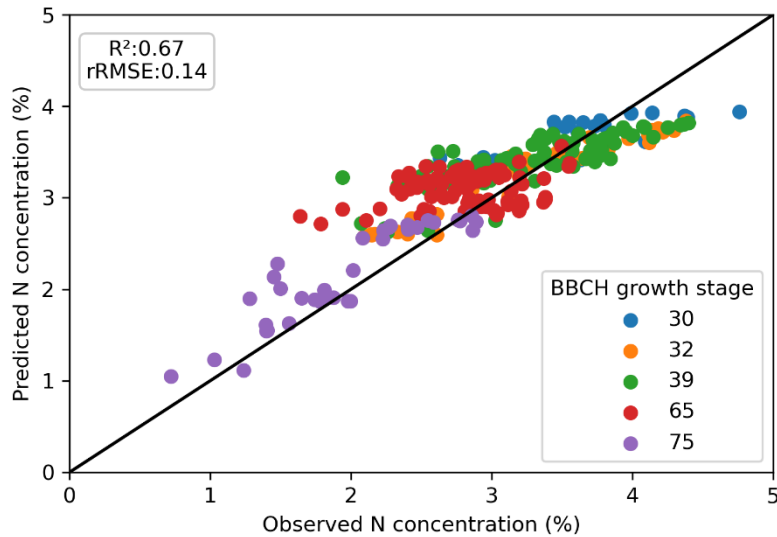
Proceedings of the 15th International Conference on Precision Agriculture
June 26-29, 2022, Minneapolis, Minnesota, United States

7

Figure 4, Plot of predicted vs observed N leaves concentration using the average of the distribution map.

Nitrogen growth curve

Trials have been followed from tillering to maturity. Figure 5 illustrates an example of the evolution of the leaf nitrogen concentration distribution for one well fertilized object of the 21-F trial. We can notice that the interquartile, i.e. percentile 75 and 25 are deviating from each other at flowering around 1500 degree days, and are merging during the maturity stages.
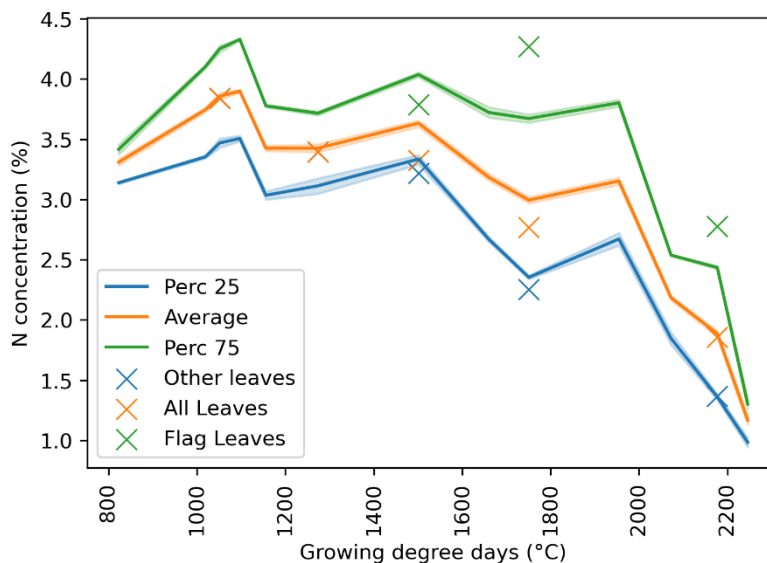

Figure 5, Nitrogen growth curve of one well fertilized object (Trial 21-F). Lines represent statistics from the nitrogen distribution, transparent colors refer to their standard deviations and crosses refer to values measured in the laboratory.

Discussion

Nitrogen map as visualization tool

In this work, a new methodology was proposed to model nitrogen maps at the pixel level. Reflectance measured by a spectroscopy sensor is a complex measure considering a wide diversity of elements such as plant physiology, plant architecture, and the sun and sensor

Proceedings of the 15th International Conference on Precision Agriculture
June 26-29, 2022, Minneapolis, Minnesota, United States

8

directions. Considering this complexity, small patches were drawn on flag leaves and on the others, while paying attention to select the most possible heterogeneous zones representing diverse situations. Whereas reflectance is influenced by viewing angles, some vegetation indices are stable across viewing angles (Lu et al., 2019). Therefore, some vegetation indices were chosen to help smoothing the nitrogen map against the huge diversity of situations encountered in an image. Growing degree days after sowing played the major role in the model, which represents 40% of the feature importance of the random forest. Unfortunately, that feature might also be responsible for flattening the point clouds for BBCH 30, 32 and 39 in Figure 4. This has the effect of gathering values around the mean and thus over-estimate low nitrogen objects and under-estimate high nitrogen objects. With a R² of 0.73, the random forest was the most suitable model to build coherent nitrogen maps. A nitrogen concentration gradient can be observed: lower leaves demonstrated lower values than upper leaves.

Several aspects are limiting the study, which makes the curve along the season broken (Figure 5). Firstly, a single nitrogen value was associated with many patches of an image, whereas nitrogen is not evenly distributed in the plant. Then, the estimation of nitrogen concentration using remote sensing is subject to discussion as mentioned by (Kattenborn et al., 2019). It is argued that pigment concentration primarily reflects leaf dry mass and not pigment variation itself. Next, there is a lack of data for the dates with no reference measurements. Finally, the pre-process is also a source of error and more specifically the registration method which sometimes yields aberrant local deformations (Dandrifosse et al., 2021).

Nitrogen partitioning in wheat

The nitrogen distribution of the observed scene was rarely computed in previous studies, and yet it is a great visualization object and seems a very good provider of information. It brought an improvement for nitrogen concentration determination of flag leaves and the other leaves (Table 2). Its dynamic is also of great interest (Figure 5). The observed interquartile widening and narrowing are consistent with the wheat physiology and more specifically with the remobilization process that occurs from anthesis (Martre et al., 2003).

Conclusion and perspectives

This study proposed a methodology to compute nitrogen maps at the pixel scale. Machine learning algorithms were trained on small patches combining features from multispectral images with laboratory nitrogen concentration measurements of flag leaves and the other leaves. The random forest yielded the best result on the validation dataset with a rRMSE of 0.12. It provides good visual nitrogen maps from which the distribution of nitrogen concentration can be extracted. Finally, the average nitrogen concentration in flag leaves and in the other leaves were best estimated with the percentile 75 and 25 of the nitrogen distribution respectively. This new methodology still needs improvements but is of great potential for further work about nitrogen distribution and remobilization. It could be fused with a height map to study the distribution of the nitrogen concentration as a function of the height of the leaf in the canopy.

References

Barnes, E. M., Clarke, T. R., Richards, S. E., Colaizzi, P. D., Haberland, J., Kostrzewski, M., Waller, P., Choi, C., Riley, E., Thompson, T., Lascano, R. J., Li, H., & Moran, M. S. (2000). Coincident detection of crop water stress, nitrogen status and canopy density using ground-based multispectral data. *Proceedings of the Fifth International Conference on Precision Agriculture*.

Barraclough, P. B., Lopez-Bellido, R., & Hawkesford, M. J. (2014). Genotypic variation in the uptake, partitioning and remobilisation of nitrogen during grain-filling in wheat. *Field Crops Research*, *156*, 242–248. https://doi.org/10.1016/j.fcr.2013.10.004

Proceedings of the 15th International Conference on Precision Agriculture
June 26-29, 2022, Minneapolis, Minnesota, United States

9

Cammarano, D., Fitzgerald, G., Casa, R., & Basso, B. (2014). Assessing the Robustness of Vegetation Indices to Estimate Wheat N in Mediterranean Environments. *Remote Sensing*, *6*(4), 2827–2844. https://doi.org/10.3390/rs6042827

Carlier, A., Dandrifosse, S., Dumont, B., & Mercatoris, B. (2022). Wheat Ear Segmentation Based on a Multisensor System and Superpixel Classification. *Plant Phenomics*, *2022*. https://doi.org/10.34133/2022/9841985

Cormier, F., Foulkes, J., Hirel, B., Gouache, D., Moënne-Loccoz, Y., & Le Gouis, J. (2016). Breeding for increased nitrogen-use efficiency: A review for wheat (*T. aestivum* L.). *Plant Breeding*, *135*(3), 255–278. https://doi.org/10.1111/pbr.12371

Dandrifosse, S., Bouvry, A., Leemans, V., Dumont, B., & Mercatoris, B. (2020). Imaging Wheat Canopy Through Stereo Vision: Overcoming the Challenges of the Laboratory to Field Transition for Morphological Features Extraction. *Frontiers in Plant Science*, *11*, 96. https://doi.org/10.3389/fpls.2020.00096

Dandrifosse, S., Carlier, A., Dumont, B., & Mercatoris, B. (2021). Registration and Fusion of Close-Range Multimodal Wheat Images in Field Conditions. *Remote Sensing*, *13*(7), 1380. https://doi.org/10.3390/rs13071380

Dandrifosse, S., Carlier, A., Dumont, B., & Mercatoris, B. (2022). In-Field Wheat Reflectance: How to Reach the Organ Scale? *Sensors*, *22*(9), 3342. https://doi.org/10.3390/s22093342

Dandrifosse, S., Ennadifi, E., Carlier, A., Gosselin, B., Dumont, B., & Mercatoris, B. (2022). Deep Learning for Wheat Ear Segmentation and Ear Density Measurement: From Heading to Maturity. *(Under Review)*.

Gitelson, A. A., Gritz †, Y., & Merzlyak, M. N. (2003). Relationships between leaf chlorophyll content and spectral reflectance and algorithms for non-destructive chlorophyll assessment in higher plant leaves. *Journal of Plant Physiology*, *160*(3), 271–282. https://doi.org/10.1078/0176-1617-00887

Gitelson, A., & Merzlyak, M. N. (1994). Quantitative estimation of chlorophyll-a using reflectance spectra: Experiments with autumn chestnut and maple leaves. *Journal of Photochemistry and Photobiology B: Biology*, *22*(3), 247–252. https://doi.org/10.1016/1011-1344(93)06963-4

Hawkesford, M. J., & Riche, A. B. (2020). Impacts of G x E x M on Nitrogen Use Efficiency in Wheat and Future Prospects. *Frontiers in Plant Science*, *11*. Scopus. https://doi.org/10.3389/fpls.2020.01157

Jay, S., Gorretta, N., Morel, J., Maupas, F., Bendoula, R., Rabatel, G., Dutartre, D., Comar, A., & Baret, F. (2017). Estimating leaf chlorophyll content in sugar beet canopies using millimeter- to centimeter-scale reflectance imagery. *Remote Sensing of Environment*, *198*, 173–186. https://doi.org/10.1016/j.rse.2017.06.008

Kattenborn, T., Schiefer, F., Zarco-Tejada, P., & Schmidtlein, S. (2019). Advantages of retrieving pigment content [μg/cm2] versus concentration [%] from canopy reflectance. *Remote Sensing of Environment*, *230*, 111195. https://doi.org/10.1016/j.rse.2019.05.014

Lu, N., Wang, W., Zhang, Q., Li, D., Yao, X., Tian, Y., Zhu, Y., Cao, W., Baret, F., Liu, S., & Cheng, T. (2019). Estimation of Nitrogen Nutrition Status in Winter Wheat From Unmanned Aerial Vehicle Based Multi-Angular Multispectral Imagery. *Frontiers in Plant Science*, *10*. https://www.frontiersin.org/article/10.3389/fpls.2019.01601

Martre, P., Porter, J. R., Jamieson, P. D., & Triboï, E. (2003). Modeling Grain Nitrogen Accumulation and Protein Composition to Understand the Sink/Source Regulations of Nitrogen Remobilization for Wheat. *Plant Physiology*, *133*(4), 1959–1967. https://doi.org/10.1104/pp.103.030585

Padilla, F. M., Gallardo, M., Peña-Fleitas, M. T., de Souza, R., & Thompson, R. B. (2018). Proximal Optical Sensors for Nitrogen Management of Vegetable Crops: A Review. *Sensors*, *18*(7), 2083. https://doi.org/10.3390/s18072083

Prey, L., & Schmidhalter, U. (2019). Sensitivity of Vegetation Indices for Estimating Vegetative N Status in Winter Wheat. *Sensors*, *19*(17), 3712. https://doi.org/10.3390/s19173712

Proceedings of the 15ᵗʰ International Conference on Precision Agriculture
June 26-29, 2022, Minneapolis, Minnesota, United States

10

Reynolds, M., Chapman, S., Crespo-Herrera, L., Molero, G., Mondal, S., Pequeno, D. N. L., Pinto, F., Pinera-Chavez, F. J., Poland, J., Rivera-Amado, C., Saint Pierre, C., & Sukumaran, S. (2020). Breeder friendly phenotyping. *Plant Science, 295,* 110396. https://doi.org/10.1016/j.plantsci.2019.110396

Roujean, J.-L., & Breon, F.-M. (1995). Estimating PAR absorbed by vegetation from bidirectional reflectance measurements. *Remote Sensing of Environment*, *51*(3), 375–384. https://doi.org/10.1016/0034-4257(94)00114-3

Verrelst, J., Malenovský, Z., Van der Tol, C., Camps-Valls, G., Gastellu-Etchegorry, J.-P., Lewis, P., North, P., & Moreno, J. (2019). Quantifying Vegetation Biophysical Variables from Imaging Spectroscopy Data: A Review on Retrieval Methods. *Surveys in Geophysics*, *40*(3), 589–629. https://doi.org/10.1007/s10712-018-9478-y

Weiss, M., Jacob, F., & Duveiller, G. (2020). Remote sensing for agricultural applications: A meta-review. *Remote Sensing of Environment*, *236*, 111402. https://doi.org/10.1016/j.rse.2019.111402

Proceedings of the 15th International Conference on Precision Agriculture
June 26-29, 2022, Minneapolis, Minnesota, United States

11